analytical chemistry

Article

Cite This: Anal. Chem. XXXX, XXX, XXX−XXX

pubs.acs.org/ac

Cu/Mn Double-Doped CeO_2 Nanocomposites as Signal Tags and Signal Amplifiers for Sensitive Electrochemical Detection of Procalcitonin

Zhe-Han Yang,[†,‡] Shirong Ren,[†] Ying Zhuo,[†] Ruo Yuan,*[,†] and Ya-Qin Chai*[,†]

[†]Key Laboratory of Luminescence and Real-Time Analytic Chemistry, Ministry of Education, College of Chemistry and Chemical Engineering, Southwest University, Chongqing 400715, People's Republic of China

[‡]Chongqing Key Laboratory of Catalysis and New Environmental Materials, College of Environment and Resources, Chongqing Technology and Business University, Chongqing, 400067, China

Supporting Information

ABSTRACT: Nanomaterials themselves as redox probes and nanocatalysts have many advantages for electrochemical biosensors. However, most nanomaterials with excellent catalytic activity cannot be directly used as redox probe to construct electrochemical biosensor because the redox signal of these nanomaterials can only be obtained in strong acid or alkali solution at high positive or negative potential, which greatly limits their applications in biologic assay. In this study, Cu/Mn double-doped CeO_2 nanocomposite (CuMn-CeO_2) was synthesized to use as signal tags and signal amplifiers for the construction of electrochemical immunosensor for sensitive assay of procalcitonin (PCT). Herein, CuMn-CeO_2 not only possesses excellent catalytic activity toward H_2O_2 for signal amplification, but also can be directly used as redox probe for electrochemical signal readout achieved in neutral mild buffer solution at low positive potential. Importantly, since doping Cu, Mn into CeO_2 lattice structure can generate extra oxygen vacancies, the redox and catalytic performance of obtained CuMn-CeO_2 was much better than that of pure CeO_2, which improves the performance of proposed immunosensor. Furthermore, CuMn-CeO_2 can be implemented as a matrix for immobilizing amounts of secondary antibody anti-PCT by forming ester-like bridging between carboxylic groups of Ab_2 and CeO_2 without extra chemical modifications, which greatly simplifies the preparative steps. The prepared immunosensor exhibited a wide linear range of 0.1 pg mL^{-1} to 36.0 ng mL^{-1} with a low detection limit of 0.03 pg mL^{-1}. This study implements nanomaterial themselves as redox probes and signal amplifiers and paves a new way for constructing electrochemical immunosensor.

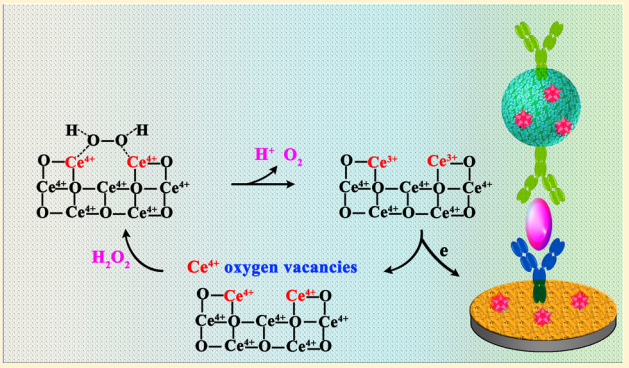

Over the past 10 years, many attempts have been made to amplify detectable signal for enhancing the sensitivity of electrochemical biosensor.[1−3] As a result, various signal amplification strategies have been explored such as enzyme catalysis amplification,[4,5] nucleic acid amplification technology,[6] and molecular conversion amplification,[7] and so on. Alternatively, nanomaterials-based signal amplification has been widely used in the construction of biosensor because of their large specific surface rate, catalytic property, and good biocompatibility.[8] Initially, nanomaterials for signal amplification depends on their large specific surface rate which can increase loading amount of the biomolecules.[9,10] Recently, nanomaterials with catalytic activity are introduced into the construction of electrochemical biosensor, in which nanomaterial can catalyze corresponding substrate to accelerate electron transfer for signal amplification.[11,12] Moreover, redox-active nanomaterials are also prepared for constructing electrochemical biosensors. Compared with other's biosensors requiring labeling redox probe, the detectable signals of these biosensors are directly originated from the nanomaterials.[13,14] Very recently, our group synthesized Au-nanoparticles-functionalized Cu(II)-MOF with catalytic and redox properties for developing an electrochemical biosensor, in which the electrochemical signal of this biosensor can be directly originated from electron transfer from Cu(II)-MOFs to Cu(I)-MOFs and amplified through catalyzing glucose oxidation by Cu(II)-MOFs itself with accelerating electron transfer.[15] Nanomaterials with catalytic and redox properties for the construction of electrochemical biosensors possess obvious advantages. On one hand, the detectable signal can be directly originated from the nanomaterials that can avoid introduction of traditional redox probe, thus, simplifying the preparative steps of biosensors. On the other hand, the signal can be

Received: August 29, 2017
Accepted: November 23, 2017

DOI: 10.1021/acs.analchem.7b03502
Anal. Chem. XXXX, XXX, XXX−XXX

Scheme 1. Schematic Illustration of the Electrochemical Immunosensor and a Proposed Mechanism of the Signal Amplification Strategy

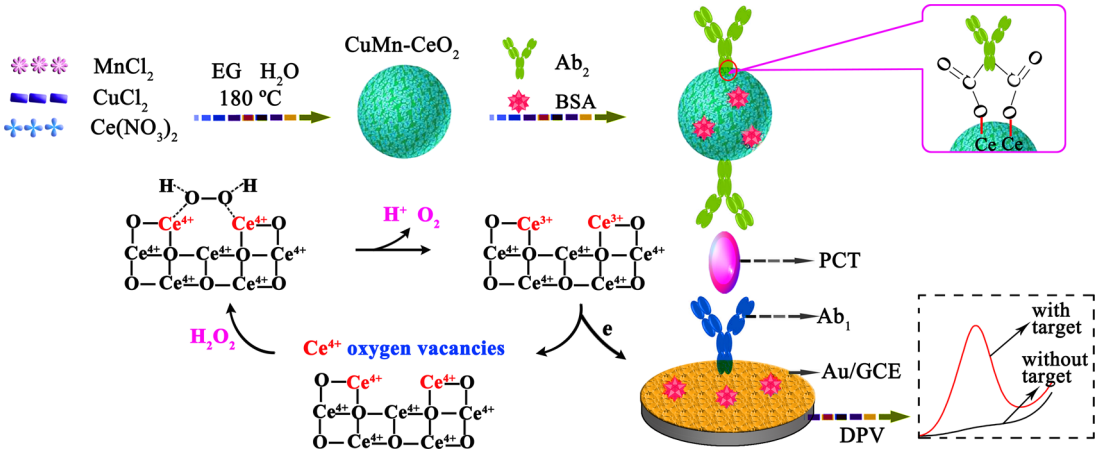

amplified by nanomaterials themselves for their catalytic properties, improving the sensitivity of biosensors. However, most nanomaterials with excellent catalytic activity cannot be directly used as redox probes to construct electrochemical biosensors because the redox signal of these nanomaterials can only be obtained in strong acid or alkali solution at high positive or negative potential, which greatly limits their applications in biologic assay.

Metal oxides nanostructures have attracted increasing attention in electrochemical biosensors due to their functional biocompatibility, unique electrical and catalytic properties.[16] Specially, metal oxides possess special surface mixed-valence properties that make it a promising material to act as a redox couple for the fabrication of electrochemical biosensors.[17] However, to date, using a metal oxide as a redox probe is rarely reported in electrochemical biosensors because the redox signal of most metal oxides must be detected in strong acid or alkali solution which limits their applications. Cerium oxide (CeO_2), one of the rare earth metal oxides, simultaneously exists Ce^{3+} and Ce^{4+} oxidation states on the lattice surface.[18−22] This unique structure endows CeO_2 with unique catalytic properties and it can be improved by introducing dopants. For example, studies of Ti-, Zr-, and Hf-doped CeO_2 reported by Nolan et al. have shown that the doped surfaces have better catalytic reactivity to CO adsorption than the undoped ones.[23] Zhang group prepared NiO-impregnated CeO_2 nanorods as a low-temperature catalyst for the NH_3-SCR of NO.[24] In the above cases, the catalytic activities of CeO_2 are improved because the oxygen vacancy formation energy can be decreased after introducing dopants, resulting in the generation of extra oxygen vacancies.[25] The dual oxidation state Ce^{3+}/Ce^{4+} on the surface of CeO_2 also endows it with a redox property. In our previous work, we found that the redox signal of CeO_2 can be detected in neutral mild buffer solutions at about 0.45 V; however, the signal is too weak to be used as probes for biosensors.[26] Therefore, it is important to search a method that can enhance the redox signal of CeO_2 for constructing highly sensitive biosensors.

In present work, by doping Cu/Mn into CeO_2 lattice structure, double-doped CeO_2 nanocomposites (CuMn-CeO_2) were prepared to propose an amplified electrochemical immunosensor for sensitive detection of procalcitonin (PCT). Since Cu and Mn simultaneously were doped into CeO_2 lattice structure, the extra oxygen vacancies were generated, endowing CuMn-CeO_2 with a superior redox performance and a better catalytic activity. As a result, CuMn-CeO_2 presented several advantages in the construction of electrochemical immunosensor. First, the electrochemical signal directly originated from the CuMn-CeO_2 in neutral mild buffer solutions at low positive potential, avoiding introduction of extra traditional redox probes. Second, the electrochemical signal was greatly amplified in the presence of H_2O_2 because of the high catalytic activity of CuMn-CeO_2 toward H_2O_2. Third, CuMn-CeO_2 with a large special surface area and a good biocompatibility was implemented as the matrix for immobilizing amounts of antibody (Ab_2) through chemical absorption between carboxylic groups of Ab_2 and CeO_2 by ester-like bridging.[27] This method demonstrates that CuMn-CeO_2 themselves can be simultaneously implemented as redox probes, signal amplifiers and matrixes in the construction of immunosensors, which greatly simplifies the preparative steps (Scheme 1).

EXPERIMENTAL SECTION

Materials and Apparatus. PCT antigens achieved from huamn, monoclonal primary antibody anti-PCT (Ab_1) and monoclonal tracer secondary antibody anti-PCT (Ab_2) were achieved from Ye Xiang Bio. Co. Ltd. (Hangzhou, China). The cerium nitrate hexahydrate ($Ce(NO_3)_3{\cdot}6H_2O$, copper chloride ($CuCl_2{\cdot}2H_2O$), manganese chloride ($MnCl_2$), polyvinylpyrrolidone (PVP), and ethylene glycol (EG) were obtained from Sinopharm Chemical Reagent Co. Ltd. (Shanghai, China). Bovine serum albumins (BSA) and gold chloride ($HAuCl_4{\cdot}4H_2O$) were purchased from Sigma-Aldrich Chem. Co. (St. Louis, MO, U.S.A.). Human real serum samples obtained from the Da Ping Hospital (Chongqing, China).

Morphologies of the prepared nanocomposite were characterized by the scanning electron microscope (SEM, S-4800, Hitachi, Japan), X-ray photoelectron spectroscopy (XPS) measurements were carried out using a VG Scientific ESCALAB 250 spectrometer (Thermoelectricity Instruments, U.S.A.) and Raman measurements were conducted with a Renishaw 2400 laser Raman microscope equipped with a 532 nm (Renishaw, U.K.). Electrochemical measurements were conducted by a conventional three-compartment electrochemical cell and CHI 660D electrochemical workstation (Shanghai Chenhua instrument, China).

Preparation of CuMn-CeO_2 Nanocomposites. CuMn-CeO_2 nanocomposites were prepared according to previous

DOI: 10.1021/acs.analchem.7b03502
Anal. Chem. XXXX, XXX, XXX−XXX

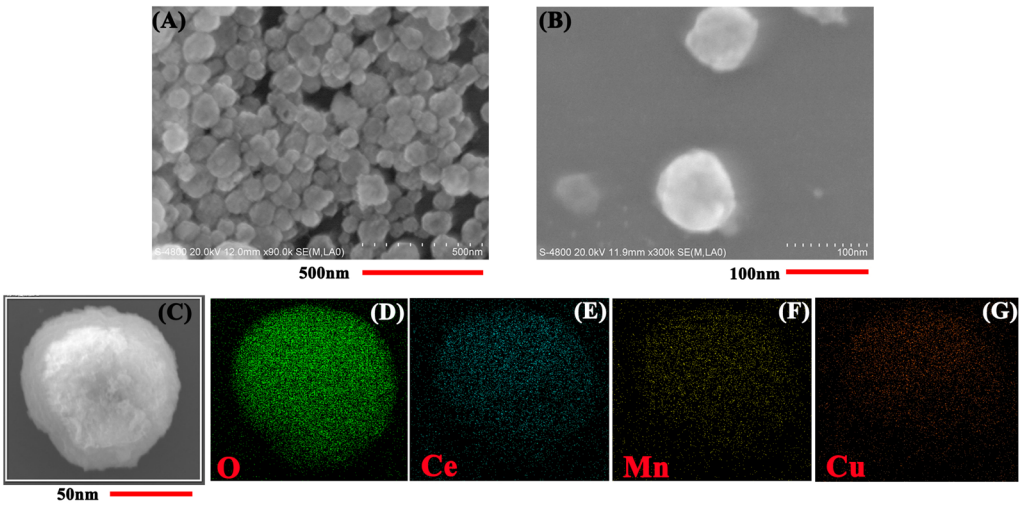

Figure 1. SEM images with different magnifications of the CuMn-CeO_2 (A, B). EDS-mapping images of an individual nanosphere (C): O (green, D), Ce (blue, E), Mn (yellow, F) and Cu (red, G).

method with a little modification.[28] First, 200 mg of PVP and 500 mg of $Ce(NO_3)_3{\cdot}6H_2O$ were added into 28 mL of EG, and stirred for 30 min at room temperature. Second, 1 mL of 20 mg mL^{-1} $CuCl_2{\cdot}2H_2O$ and 1 mL of 20 mg mL^{-1} $MnCl_2$ solution were introduced into the above obtained solution, and then transferred into a Teflon-lined autoclave of 50 mL capacity and heated for 8 h at 180 °C. After cooling to room temperature, the prepared products were collected and washed with doubly distilled water and absolute alcohol several times. Finally, the products were dried at 60 °C and then calcined at 450 °C at 1 °C min^{-1} for 1 h.

Preparation of Ab_2 Bioconjugates. First, 100 μL of Ab_2 solution (2.2 mg mL^{-1}) was added into 2 mL of CuMn-CeO_2 and gently stirred for 12 h at 4 °C. Then 80 μL of BSA solution was introduced into above solution and continually stirred for 2 h at 4 °C, making Ab_2 and BSA-coated CuMn-CeO_2 (BSA/Ab_2/CuMn-CeO_2) with formation of Ab_2 bioconjugates collected by centrifugation at 4 °C. After that, the prepared Ab_2 bioconjugate was dispersed in PBS (pH 7.0) and stored at 4 °C for further use.

Immunosensor Fabrication Process. A mirror GCE was obtained by carefully polishing GCE with 0.05 and 0.3 μm Al_2O_3 powder on a fine abrasive paper sequentially and then ultrasonicated in doubly distilled water for 20 s and repeated the procedure twice. The pretreated GCE was immersed into 1% (w/w) $HAuCl_4{\cdot}4H_2O$ solution to obtain AuNP film by using electrochemical deposition under −0.2 V for 30 s. Subsequently, the formed AuNP modified GCE (Au/GCE) was incubated with 15 μL Ab_1 (24 μg mL^{-1}) at 4 °C for 12 h. Successively, the resulting modified GCE was blocked with 1 mg mL^{-1} BSA at room temperature for 1 h. On the basis of the sandwich format, the modified GCE was incubated with PCT samples with different concentrations for 40 min at 37 °C, followed by incubating with 15 μL of Ab_2 bioconjugate solution for immune reaction at 37 °C for 30 min. Subsequently, the prepared immunosensor was washed with PBS (pH 7.0) to remove unbound Ab_2 bioconjugates. The electrochemical signal was carried out in PBS (pH 7.0) with 25.0 mM H_2O_2, which gave the quantitative criteria for electrochemical detection of PCT.

Electrochemical Measurements. Electrochemical experiments were carried out by a standard three-electrode system. DPV measurements were performed in 2 mL of 0.1 M PBS (pH 7.0) at room temperature with 25.0 mM H_2O_2, and the parameters applied were 50 mV/s sweeping rate, 20 mV pulse amplitude, 50 ms pulse width, 2 s pulse period, and a voltage range from 0.2 to 0.6 V. CV measurements were performed in 5.0 mM $[Fe(CN)_6]^{3-/4-}$ with a scanning potential from −0.2 to 0.6 V at a scan rate of 50 mV/s.

RESULTS AND DISCUSSION

Characteristics of the CuMn-CeO_2. The morphologies of CuMn-CeO_2 nanocomposites were characterized by SEM. As shown in Figure 1A, the CuMn-CeO_2 showed uniform-size nanospheres and a rough surface of the nanosphere can be observed from a close-up view SEM image, indicating that many small nanoparticles exists on the surface (Figure 1B). Moreover, elemental mapping analysis using energy dispersive spectroscopy (EDS) conducted on a single CuMn-CeO_2 confirms the occurrence of homogeneous distributions of Ce, Cu, Mn, and O (Figure 1D-G).

Raman spectroscopies can provide more information on the surface of nanocomposites. The Raman spectra of CeO_2 and CuMn-CeO_2 excited at 532 nm with 10% laser power and the image is showed in Figure 2. For the CeO_2 sample, a main Raman band around 462 cm^{-1} can be observed, which is related to the triply degenerate F_{2g} Raman active mode of the CeO_2 fluorite structure (curve a).[29] For the CuMn-CeO_2 sample, the

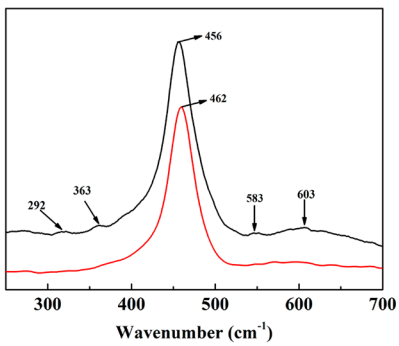

Figure 2. Raman spectra for CeO_2 nanospheres before (red line) and after (black line) doping with Cu/Mn.

DOI: 10.1021/acs.analchem.7b03502
Anal. Chem. XXXX, XXX, XXX−XXX

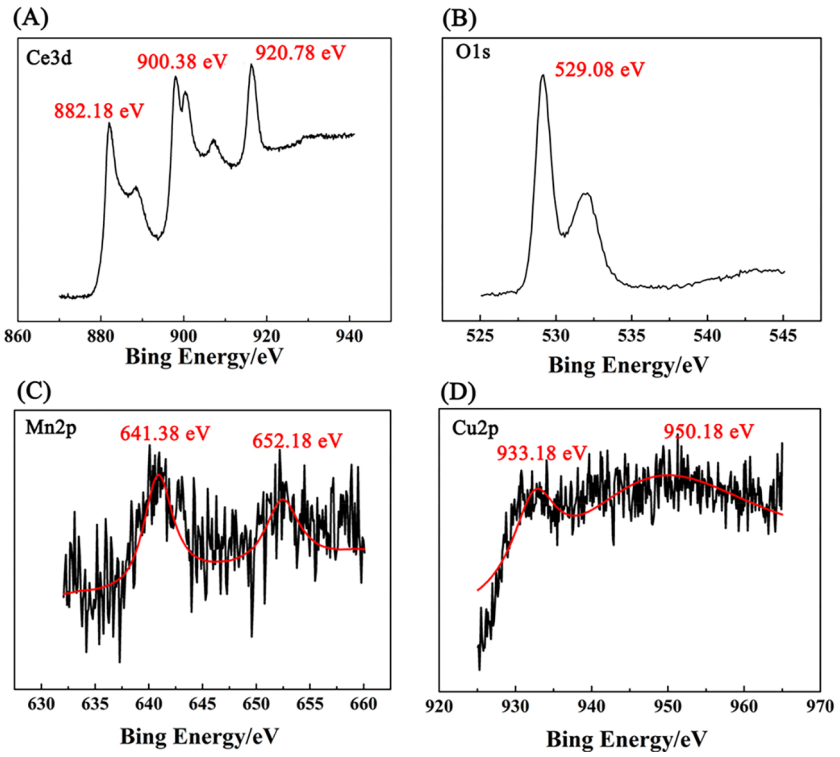

Figure 3. XPS spectra for the CuMn-CeO_2: Ce 3d (A), O 1s (B), Mn 2p (C), Cu 2p (D).

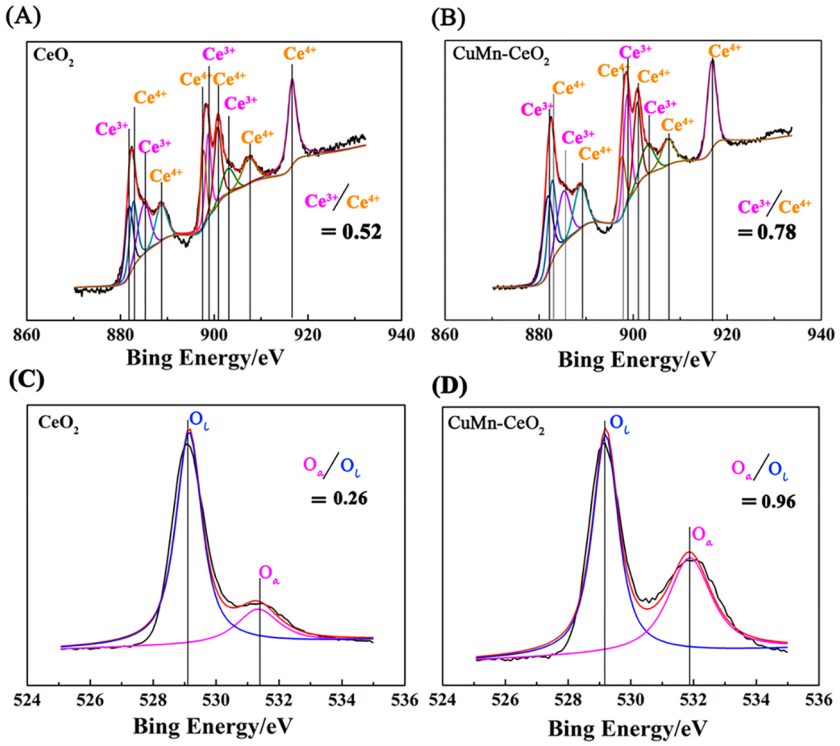

Figure 4. Ce 3d XPS spectra of the pure CeO_2 (A) and CuMn-CeO_2 (B); O 1s XPS spectra of the pure CeO_2 (C) and CuMn-CeO_2 (D).

band ascribed to the F_{2g} mode of CeO_2 shifts to lower frequency at about 456 cm^{-1} and the width of peak increases. The above phenomena implies that defects in the lattice structure of the CeO_2 after doping with Cu/Mn have occurred, as it was previously reported that lattice defects in CeO_2 leads to a shifted peak position to lower frequency.[30] In addition, obvious bands are observed at 292, 603, 363, and 583 cm^{-1}, which is related to the formation of oxygen vacancies when doping of Cu^{2+}/Mn^{2+} on the lattice site Ce^{4+} ion. The above phenomena confirms that CuMn-CeO_2 exists extra oxygen vacancies.

XPS is a powerful technique that can provide more information on elemental analysis of CuMn-CeO_2. As seen from Figure 3, The Ce 3d triple (882.18, 900.38, and 920.78

DOI: 10.1021/acs.analchem.7b03502
Anal. Chem. XXXX, XXX, XXX−XXX

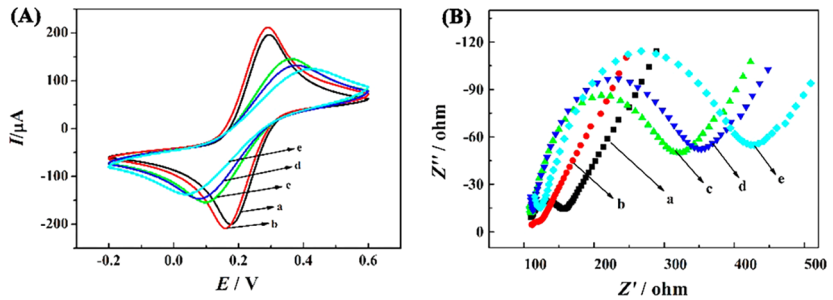

Figure 5. CV (A) and EIS (B) of different modified electrodes in PBS buffer containing 5.0 mM $[Fe(CN)_6]^{3-/4-}$: (a) bare GCE; (b) Au/GCE; (c) Ab_1/Au/GCE; (d) BSA/Ab_1/Au/GCE; (e) PCT/BSA/Ab_1/Au/GCE.

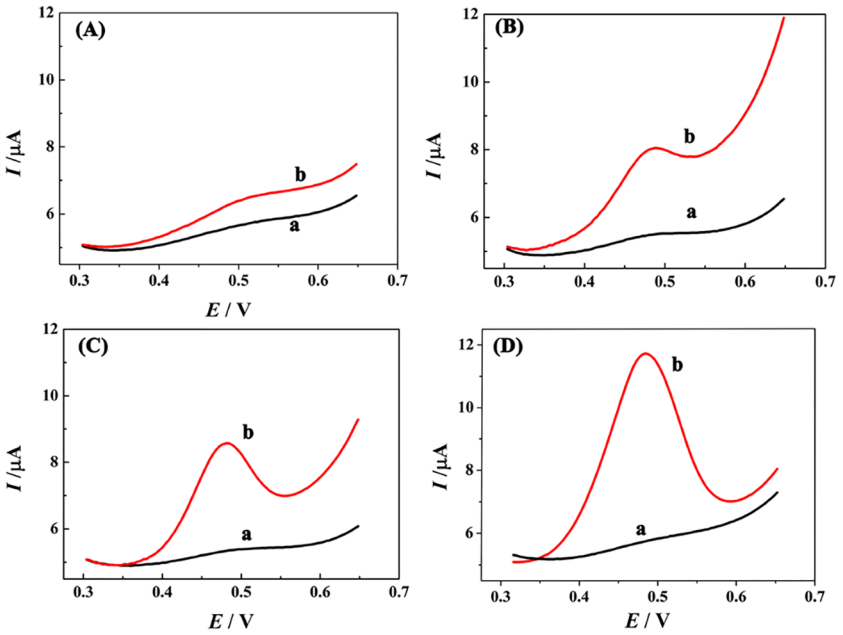

Figure 6. DPV responses of the proposed immunosensor incubated with 18.0 ng/mL PCT using Ab_2/BSA/CeO_2 (A), Ab_2/BSA/Cu-CeO_2 (B), Ab_2/BSA/Mn-CeO_2 (C), Ab_2/BSA/CuMn-CeO_2 (D) as tracers in absence of H_2O_2 (curve a) and in the presence of 25.0 mM H_2O_2 (curve b).

eV, Figure 3A) and the O 1s (529.08 eV; Figure 3 B) confirms the presence of CeO_2. The peak at 652.18 and 934.18 eV can be assigned to Mn 2p (Figure 3C) and Cu 2p (Figure 3D), respectively, which confirms that Cu/Mn are successfully doped into CeO_2.

To further obtain information on the chemical state distributions on the surface of the CeO_2 before and after doping with Cu/Mn. The two oxidation states content ratios of pure CeO_2 (Figure 4A) and CuMn-CeO_2 (Figure 4B) were investigated. The Ce XPS spectra is labeled for the Ce^{4+} and Ce^{3+} chemical species, which were fitted by Gaussian distributions with different peak positions and areas.[31,32] Binding energies of Ce^{4+} are founded at 900.5, 906.7, 916.6, 882.3, 888.8, and 897.6 eV. Similarly peaks are marked at 898.5, 903.1, 881.8, and 885.1 eV represented Ce^{3+}. Compared with pure CeO_2, the Ce^{3+}/Ce^{4+} content ratio on the surface of CuMn-CeO_2 was increased from 0.52 to 0.78. Therefore, doping Cu, Mn into the CeO_2 can make the Ce^{3+}/Ce^{4+} content ratio increase, and thus, it has been demonstrated that an increase of the Ce^{3+} species on the surface of CuMn-CeO_2, improving the redox potential and the catalytic activities of CuMn-CeO_2.

As mention above, doping Cu/Mn into CeO_2 lattice structure will lead to extra oxygen vacancies. To confirm this issue, the peak deconvolutions of the O 1s XPS spectraof the surfaces of the CeO_2 and CuMn-CeO_2, including the surface-adsorbed oxygen (O_a) and the lattice oxygen (O_l) are investigated. Herein, O_a represents surface-adsorbed belonging to the defect oxide or hydroxyl-like group, corresponding to a higher binding energy. The binding energy of O_a is about 531.5 eV and the binding energy of O_l is about 529.2 eV.[33−35] The surface oxygen vacancy change can be represented by using the O_a/O_l ratio. As shown in Figure 4C,D, the O_a/O_l ratio of the pure CeO_2 and the CuMn-CeO_2 is 0.26 and 0.96, respectively, which indicates that the CuMn-CeO_2 can generate more active O_a species.

Characteristics of the Fabrication Steps of Modified GCE. CV measurements were constructed in 5.0 mM of $[Fe(CN)_6]^{3-/4-}$ to fabricate the electrode surface at each step. The experimental results were shown in Figure 5A. Compared with the bare GCE (curve a), the peak current value of AuNP modified GCE (Au/GCE, curve b) remarkably increases because AuNP layer can increase the charge transfer rate and enhance the electrode effective area. After the Ab_1 was immobilized on Au/GCE surface, a decrease peak current is observed due to protein hinder electron transfer from solution to electrode surface (curve c). After incubating with BSA, peak current further decrease (curve d). When PCT antigen was

DOI: 10.1021/acs.analchem.7b03502
Anal. Chem. XXXX, XXX, XXX−XXX

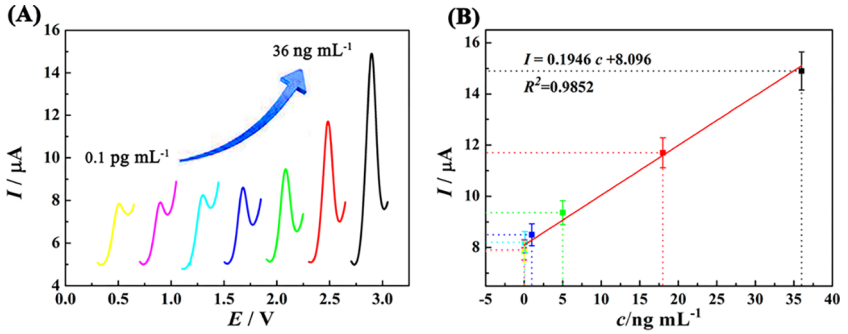

Figure 7. DPV responses of the proposed immunosensors after incubation with various concentrations of PCT (A). Calibration curve of the intensity current of the immunosensor with Ab_2/BSA/CuMn-CeO_2 (B).

Table 1. Comparisons of Proposed Method with Other Reported Nanomaterials-Based Electrochemical Immunosensors

nanomaterials	methods	linear ranges	detection limit	reference
PtNPs	chronocoulometry	1 pg mL^{-1} to 100 ng mL^{-1}	1 pg mL^{-1}	36
Fe_3O_4@MnO_2@Pt	chronocoulometry	0.5 pg mL^{-1} to 20 ng mL^{-1}	0.16 pg mL^{-1}	37
MOF	DPV	1.0 ng mL^{-1} to 400 ng mL^{-1}	0.2 ng mL^{-1}	38
RGO-ph-AuNP	SWV	0.1 pg mL^{-1} to 0.15 ng mL^{-1}	0.1 pg mL^{-1}	39
CuMn-CeO_2	DPV	0.1 pg mL^{-1} to 36.0 ng mL^{-1}	0.03 pg mL^{-1}	this work

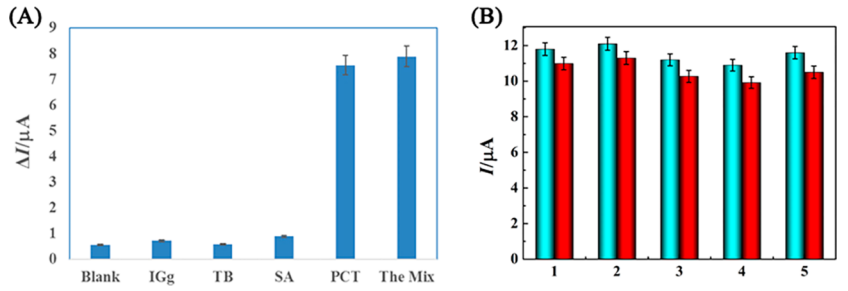

Figure 8. (A) DPV current response of five electrochemical immunosensors (blue pillar) and obtained after 25 days (red pillar). (B) Specificity of the electrochemical immunosensor investigated by DPV measurement in 2 mL of 0.1 M PBS (pH 7.0) at room temperature with 25.0 mM H_2O_2.

incubated, peak current also decrease, indicating that PCT antigens successfully bind to Ab_1 immobilized electrode surface (curve e). EIS measurements were also implemented to further provide information about the preparation of the immunosensor. The results were presented in Figure 5B. The curve a is the EIS response of bare GCE. Then, a decrease in the charge-transfer resistance (R_{ct}) value can be observed after electrodeposition of AuNPs on GCE (curve b) because the conductivity of AuNPs accelerate the electron transfer of the redox probe to the electrode. When the Ab_1 are immobilized onto Au/GCE surface, the R_{ct} value increase (curve c). BSA was used to block specific sites and lead to a further increase of R_{ct} (curve d). After incubated with PCT antigen, R_{ct} also increases, indicating that PCT antigens successfully bind to Ab_1 immobilized electrode surface. On the basis of above result, it could be seen that the information provided by the R_{ct} value change was agreed with that of the CV current changes, indicating that the immunosensor was successfully constructed.

Investigation of the Catalytic Performance of CuMn-CeO_2 for Signal Amplification. To demonstrate the high catalytic activity of CuMn-CeO_2 toward H_2O_2 oxidation for electrochemical signal amplification, three additional nanocomposites including CeO_2, Cu-CeO_2 and Mn-CeO_2 were investigated. The same batch immunosensors incubated with PCT (18.0 ng mL^{-1}) and then reacted with Ab_2/BSA/CeO_2, Ab_2/BSA/Cu-CeO_2, Ab_2/BSA/Mn-CeO_2, and Ab_2/BSA/CuMn-CeO_2 bioconjugates, respectively. The DPV experiments were conducted to record the result before (curve a) and after (curve b) addition H_2O_2 into test solution. Figure 6A shows that the DPV response of the immunosensor modified with Ab_2/BSA/CeO_2 bioconjugates in PBS buffer containing H_2O_2 (curve b) is higher than that of in absence of H_2O_2 (curve a), which indicated that pure CeO_2 can catalyze H_2O_2 oxidation for accelerating electro transfer from Ce^{3+} to Ce^{4+}. However, the above current responses are lower than that of the immunosensor with Ab_2/BSA/Cu-CeO_2 (Figure 6B) and Ab_2/BSA/Mn-CeO_2 bioconjugates (Figure 6C). These results should be ascribed to that the doping CeO_2 with Cu or Mn improves the catalytic performance of CeO_2. Moreover, the immunosensor with Ab_2/BSA/CuMn-CeO_2 bioconjugates (Figure 6D) exhibits the highest peak current compared with the immunosensor with the above three kinds of bioconjugates. This suggests that the catalytic performance of CeO_2 doped with bimetal elements was much better than that of CeO_2 doped with single metal element. The experimental results demonstrate that the signal amplification strategy based on CuMn-CeO_2 can be implemented to improve the sensitivity of the proposed immounsensor.

Performance of the Immunosensor. The sensitivity of the fabricated electrochemical immunosensor was investigated using PCT with various concentrations. As shown in Figure 7, the DPV peak current increases when the concentration of

DOI: 10.1021/acs.analchem.7b03502
Anal. Chem. XXXX, XXX, XXX−XXX

target PCT is raised from 0.1 pg mL^{-1} to 36.0 ng mL^{-1}, which indicates that the immobilization of Ab_2 bioconjungates on the electrode is highly dependent on the concentration of target PCT. In addition, the directly measured detection limit toward target PCT is 0.03 pg mL^{-1}, providing superior or comparable detection sensitivity compared with those reported electrochemical biosensors based on nanomaterials as catalysts (Table 1). The results demonstrated that the proposed biosensor is efficient for sensitive electrochemical detection of target PCT.

To evaluate the specificity of the proposed immunosensor for target PCT assay, three interference proteins including thrombin (TB), hemoglobin (IGg) and streptavidin (SA) were assessed. The modified electrodes incubated the three interference proteins and the target PCT were conducted by DPV under the same experimental conditions. To test the immunosensor specificity, an excessive interference protein concentration of 200 ng mL^{-1} was used. As shown in Figure 8A, DPV signals from experiments involving IGg, TB, and SA are similar to the blank control. In contrast, the DPV signal from the detection PCT (5.0 ng mL^{-1}) is about 10-fold higher than the signals of those interferences. Meanwhile, when the immunosensor incubated with the mixture solution of 5 ng mL^{-1} PCT and the three interferences (200 ng mL^{-1}), the DPV responses are almost no obvious change in comparison with the case of only PCT. These experimental results indicate the high specificity of our immunosensor for target PCT recognition and subsequent electrochemical detection.

The long-term stability experiment was also performed to evaluate the stability of the proposed immunosensor. Briefly, five of immunosensors with 18.0 ng mL^{-1} PCT were stored at 4 °C and detected every 5 days under the same experimental conditions. After 25 days, the current retained 93.2%, 93.5%, 91.7%, 91.1%, and 90.9% of their initial current values (Figure 8B), indicating that the immunosensors have a good stability.

Clinical Serum Samples Analysis. The immunosensor performances in more complex biological environment were investigated by spike and recovery experiments. Briefly, the healthy human serum sample was used to dilute a serious of concentrations of standard PCT samples. Then, the immunosensor incubated with the above samples were investigated to assess the influence of the serum samples for PCT assay. Table 2 shows the experimental result, it can be seen that the recovery

Table 2. Recovery Results of the Proposed Immunosensor in Human Serum

sample no.	added (ng mL^{-1})	found (ng mL^{-1})	recovery (%)	RSD (%)
1	0	0.002		2.12
2	0.10	0.093	93.0	8.15
3	0.50	0.49	95.0	9.33
4	1.0	1.07	107	7.29
5	10.0	9.82	98.2	9.96

is varying from 93.0% to 107% and RSDs is ranging from 7.29% to 9.96%. These results clearly suggest that our proposed immunosensor can be applied for PCT detection in complex biological samples.

CONCLUSION

In this work, a simple signal-amplified electrochemical immunosensor was proposed by using CuMn-CeO_2 as redox probes, signal amplifiers and matrixes for sensitive detection of PCT. CuMn-CeO_2 was successfully synthesized via doping Cu/Mn into CeO_2 lattice structure. It is found that double doped-CeO_2 exhibits more excellent catalytic activity than that of pure CeO_2. More importantly, CuMn-CeO_2 themselves can directly be used as redox probes and signal amplifiers, which not only avoids introduction of extra redox probes, but also improves the sensitivity of immunosensor. It is noted that this investigation provides a new redox probe and a novel nanocatalyst for constructing electrochemical biosensors. In addition, this strategy may provide a simple and sensitive method for the construction of electrochemical biosensor for monitoring biomolecules that may be related to diseases.

ASSOCIATED CONTENT

Supporting Information

The Supporting Information is available free of charge on the ACS Publications website at DOI: 10.1021/acs.analchem.7b03502.

Figure S1 showing the optimization of the H_2O_2 concentration; Figure S2 showing the XPS spectra of pure CeO_2 (PDF)

AUTHOR INFORMATION

Corresponding Authors

*Tel.: +86-23-68252277. Fax: +86-23-68253172. E-mail: yuanruo@swu.edu.cn.

*E-mail: yqchai@swu.edu.cn.

ORCID

Ruo Yuan: 0000-0003-3664-6236

Notes

The authors declare no competing financial interest.

ACKNOWLEDGMENTS

The authors are grateful for the National Natural Science Foundation of China (21775124, 21575116, 21675129,), the Fundamental Research Funds for the Central Universities (XDJK2015A002), China.

REFERENCES

(1) Miao, P.; Tang, Y.; Wang, B.; Yin, J.; Ning, L. *TrAC, Trends Anal. Chem.* **2015**, *67*, 1−15.

(2) Ball, C. S.; Light, Y. K.; Koh, C. Y.; Wheeler, S. S.; Coffey, L. L.; Meagher, R. J. *Anal. Chem.* **2016**, *88*, 3562−3568.

(3) Yang, Z. H.; Zhuo, Y.; Yuan, R.; Chai, Y. Q. *Nanoscale* **2017**, *9*, 2556−2562.

(4) Akama, K.; Shirai, K.; Suzuki, S. *Anal. Chem.* **2016**, *88*, 7123−7129.

(5) Liu, X.; Li, W.; Hou, T.; Dong, S.; Yu, G.; Li, F. *Anal. Chem.* **2015**, *87*, 4030−4036.

(6) Zhao, Y.; Chen, F.; Li, Q.; Wang, L.; Fan, C. H. *Chem. Rev.* **2015**, *115*, 12491−12545.

(7) Yang, Z. H.; Zhuo, Y.; Yuan, R.; Chai, Y. Q. *Anal. Chem.* **2016**, *88*, 5189−5196.

(8) Chen, A.; Chatterjee, S. *Chem. Soc. Rev.* **2013**, *42*, 5425−5438.

(9) Wang, F.; Liu, J. W. *Nanoscale* **2014**, *6*, 7079−7084.

(10) Ortac, I.; Simberg, D.; Yeh, Y. S.; Yang, J.; Messmer, B.; Trogler, C. W.; Tsien, R. Y.; Esener, S. *Nano Lett.* **2014**, *14*, 3023−3032.

(11) Voiry, D.; Yamaguchi, H.; Li, J.; Silva, R.; Alves, D. C. B.; Fujita, T.; Chen, M.; Asefa, T.; Shenoy, V. B.; Eda, G.; Chhowalla, M. *Nat. Mater.* **2013**, *12*, 850−855.

(12) Wei, H.; Wang, E. *Chem. Soc. Rev.* **2013**, *42*, 6060−6093.

(13) Roushani, M.; Shahdost-fard, F. *Sens. Actuators, B* **2015**, *207*, 764−771.

(14) Han, J.; Zhuo, Y.; Chai, Y. Q.; Xiang, Y.; Yuan, R. *Anal. Chem.* **2015**, *87*, 1669−1675.

DOI: 10.1021/acs.analchem.7b03502
Anal. Chem. XXXX, XXX, XXX−XXX

(15) Shen, W. J.; Zhuo, Y.; Chai, Y. Q.; Yuan, R. *Anal. Chem.* **2015**, *87*, 11345−11352.
(16) Shen, G. Z.; Chen, P. C.; Ryu, K.; Zhou, C. *J. Mater. Chem.* **2009**, *19*, 828−839.
(17) Chiu, C. C.; Vogt, T.; Zhao, L.; Genest, A.; Rösch, N. *Dalton Trans.* **2015**, *44*, 13778−13795.
(18) Wang, F.; Li, W.; Feng, X.; Liu, D. *Chem. Sci.* **2016**, *7*, 1867−1873.
(19) Quiroz, J.; Giraudon, J. M.; Gervasini, A.; Dujardin, C.; Lancelot, C.; Trentesaux, M.; Lamonier, J. F. *ACS Catal.* **2015**, *5*, 2260−2269.
(20) Maitarad, P.; Han, J.; Zhang, D.; Shi, L.; Namuangruk, S.; Rungrotmongkol, T. *J. Phys. Chem. C* **2014**, *118*, 9612−9620.
(21) Xu, L.; Wang, J. *Environ. Sci. Technol.* **2012**, *46*, 10145−10153.
(22) Yang, X.; Yang, L.; Lin, S.; Zhou, R. *J. Phys. Chem. C* **2015**, *119*, 6065−6074.
(23) Nolan, M. *J. Phys. Chem. C* **2009**, *113*, 2425−2432.
(24) Razzaq, R.; Zhu, H.; Jiang, L.; Muhammad, U.; Li, C.; Zhang, S. *Ind. Eng. Chem. Res.* **2013**, *52*, 2247−2256.
(25) Zhen, J. M.; Liu, D. P.; Wang, X.; Li, J. Q.; Wang, F.; Wang, Y. H.; Zhang, H. J. *Dalton Trans.* **2015**, *44*, 2425−2430.
(26) Yang, Z. H.; Zhuo, Y.; Yuan, R.; Chai, Y. Q. *Biosens. Bioelectron.* **2015**, *69*, 321−327.
(27) Lu, Z.; Karakoti, A.; Velarde, L.; Wang, W.; Yang, P.; Thevuthasan, S.; Wang, H. *J. Phys. Chem. C* **2013**, *117*, 24329−24338.
(28) Liu, W.; Liu, X.; Feng, L.; Guo, J.; Xie, A.; Wang, S.; Zhang, J.; Yang, Y. *Nanoscale* **2014**, *6*, 10693−10700.
(29) Wu, Z.; Li, M.; Howe, J.; Meyer, H. M.; Overbury, S. H. *Langmuir* **2010**, *26*, 16595−16606.
(30) Choudhury, B.; Choudhury, A. *Curr. Appl. Phys.* **2013**, *13*, 217−223.
(31) Beche, E.; Charvin, P.; Perarnau, D.; Abanades, S.; Flamant, G. *Surf. Interface Anal.* **2008**, *40*, 264−267.
(32) Wang, Z.; Qu, Z.; Quan, X.; Wang, H. *Appl. Catal., A* **2012**, *411-412*, 131−138.
(33) Cheng, K.; Liu, J.; Zhang, T.; Li, J.; Zhao, Z.; Wei, Y.; Jiang, G.; Duan, A. *J. Environ. Sci.* **2014**, *26*, 2106−2113.
(34) Gao, R.; Zhang, D.; Maitarad, P.; Shi, L.; Rungrotmongkol, T.; Li, H.; Zhang, J.; Cao, W. *J. Phys. Chem. C* **2013**, *117*, 10502−10511.
(35) Wang, Y.; Shen, B.; He, C.; Yue, S.; Wang, F. *Environ. Sci. Technol.* **2015**, *49*, 9355−9363.
(36) Dutta, G.; Nagarajan, S.; Lapidus, L. J.; Lillehoj, P. B. *Biosens. Bioelectron.* **2017**, *92*, 372−377.
(37) Wu, D.; Ma, H.; Zhang, Y.; Jia, H.; Yan, T.; Wei, Q. *ACS Appl. Mater. Interfaces* **2015**, *7*, 18786−18793.
(38) Liu, T. Z.; Hu, R.; Zhang, X.; Zhang, K. L.; Liu, Y.; Zhang, X. B.; Bai, R. Y.; Li, D.; Yang, Y. H. *Anal. Chem.* **2016**, *88*, 12516−12523.
(39) Qi, M.; Zhang, Y.; Cao, C.; Zhang, M.; Liu, S.; Liu, G. *Anal. Chem.* **2016**, *88*, 9614−9621.

DOI: 10.1021/acs.analchem.7b03502
Anal. Chem. XXXX, XXX, XXX−XXX